Journal of Applied Polymer Science

Seaweed-ZnO Composite for Better Antibacterial Properties

R. Pandimurugan, S. Thambidurai
Department of Industrial Chemistry, School of Chemical Sciences, Alagappa University, Karaikudi 630003, Tamil Nadu, India
Correspondence to: S.Thambidurai (E-mail: sthambi01@yahoo.co.in)

ABSTRACT: Brown seaweed *Padina tetrastromatica* (PTS)-Zinc oxide (ZnO) composites were prepared by chemical precipitation method. The characteristic peaks of PTS and ZnO were confirmed by Fourier transform infrared spectroscopy. X-Ray diffraction study was confirmed the formation of ZnO with hexagonal wurtzite phase. Surface morphology and particle's distribution of ZnO were characterized by scanning electron microscopy. Transmission Electron microscopy image reveals that ZnO nanorods are in the size range of 14–164 nm having uniformly blended with polysaccharide of seaweed. Ultraviolet-Visible absorption spectra indicated the sharp absorption peak at 219 nm and broad absorption peak in the 250–350 nm range. Fluorescence spectra shows the broad blue-violet emissions is around at 380–480 nm. Because of the interaction between polysaccharide and ZnO nanorods/particles, the prepared seaweed-ZnO composite exhibit better antibacterial activity than pure ZnO nanoparticles. © 2014 Wiley Periodicals, Inc. J. Appl. Polym. Sci. **2014**, *131*, 40948.

KEYWORDS: biopolymers and renewable polymers; nanoparticles; nanowires and nanocrystals; polysaccharides; X-ray

Received 21 January 2014; accepted 1 May 2014
DOI: 10.1002/app.40948

INTRODUCTION

In recent years, ZnO nanocrystalline materials have gained great importance as they represent a class of material with new exciting properties and wide technological applications. Generally, material properties are size-dependent, and if the particle sizes of ZnO nanoparticles are reduced, the optical band gap can be improved.[1] The tunability of the properties of ZnO with the particle size may find applications in formulating new composite materials for various applications such as in polymers, fabrics, and cosmetic materials.[2–4] Among the available synthesis methods, it is well conceived that solution chemical routes are more convenient, less expensive and have general advantages such as superior uniformity and high yield of nanoparticles.[5] Currently, for size reduction purpose, various synthetic surfactant molecules like hexamine, tetraethyl ammonium bromide, cetyl trimethyl ammonium bromide, and Tetra octyl ammonium bromide were used.[6]

Polymer with some functional groups such as cyano (—CN), mercapto (—SH), and amino ($—NH_2$) groups are known to have a high affinity for metals; hence, they can be used as a protecting agent to prepare monodisperse metal nanoparticles.[7] Many polymers have been used to prepare metal–polymer nanocomposites, and it has been found that the addition of metal oxide with polymer causes property changes of either the host or the guest and envisioned the formation of a new type of inorganic–polymer nanocomposites.[8]

Nowadays, the use of antibiotics increases significantly due to heavy infections and the pathogenic bacteria becoming resistant to drugs. Seaweed is a group of marine plants abundantly available for the worldwide seashore and represent a potential source of antimicrobial substances next to the chitosan due to their diversity of secondary metabolites with antioxidant[9] and antiviral properties.[10] Antibacterial activity of seaweeds is generally assayed using extracts in various organic solvents, and the bioactive nano particles with various functional groups are isolated from the extract.[11]

Seaweeds such as brown alga *padina gymnospora* accumulate more metals in the negatively charged polysaccharides in physodes.[12] From the literature, the seaweed polysaccharides were used for preparation of metal/metal oxide nanocomposite,[13–15] but there is no available literatures related to antibacterial activity test.

In this study, it is aimed to prepare the seaweed-ZnO composite by treating *padina tetrastromatica* (PTS) seaweed with zinc cation precursor chemicals such as zinc chloride, zinc acetate, and zinc sulfate using sodium hydroxide as precipitating agent. The prepared samples were characterized by FTIR, XRD, HR-SEM, TEM, UV-Vis, and FL instrumental techniques and examined the antibacterial activity toward *Escherichia coli* (gram-negative bacteria) and *Staphylococcus aureus* (gram-positive bacteria) by disc diffusion method, and colony count method. In both antibacterial test methods, an increased antibacterial activity of seaweed-ZnO composite over ZnO was noticed.

EXPERIMENTAL

Materials

Zinc chloride (95%), zinc acetate (98%), zinc Sulfate (99.5%), and sodium hydroxide (98%), were analytical grade and purchased from Fischer Chemic Ltd, Chennai, India. Fresh seaweeds of PTS were collected from the Gulf of Mannar in the south India and washed with seawater followed by thorough washing with fresh water. The moisture was completely removed. Then, they were ground well in a mortar to get dry seaweed powder. Doubly distilled water was used throughout the experiment.

Synthesis of Seaweed-ZnO Composite

ZnO nanoparticles were prepared by treating dry powder of PTS with three zinc source materials $ZnCl_2$, Zn $(CH_3COO)_2$, and $ZnSO_4$ separately. In a 500-mL beaker, 0.5 g of dry PTS powder was mixed with 25 mL of 25% zinc chloride solution and the solution was heated at 70°C for 2 h by stirring on magnetic stirrer at atmospheric pressure. At the end of the 2 h duration, the clear solution was filtered off, and 25 mL of 25% of aqueous sodium hydroxide solution was added slowly in the clear solution. The formed precipitate was allowed to settle for 48 h, washed with doubly distilled water for several times, and finally filtered using a suction pump. The filtrate was dried in hot air oven at 110°C for 2 h and designated the sample as ZCP. The above process was repeated by replacing 25% of zinc chloride with 25% of zinc acetate and zinc sulfate and designated as ZAP and ZSP, respectively.

Characterization

Fourier transform infrared (FTIR) spectra (transmission) were recorded on a Thermo-Nicolet-380 Madison, USA model spectrum one in the range of 4000–400 cm^{-1} at room temperature. The crystallite size of the prepared samples was recorded using an X-ray diffractometer (X'Pert PRO Pan Analytical diffractometer) of Cu K_α radiation ($\lambda = 0.15406$ nm) with the scanning rate of 0.01°/step. The SEM images of the samples were depicted using Quanta FEG-250 HR-SEM. TEM image was obtained on a (PHILIPS CM200) transmission electron microscope at an acceleration voltage of 200 kV. The prepared nanocomposite were dispersed in ethanol solution and then transferred onto Cu/lacey carbon TEM grids. The optical absorption spectra were taken on a UV–visible spectrophotometer (2401 PC model; Shimadzu, Kyoto, Japan) in the wavelength range of 200–800 nm. The fluorescence spectra were recorded in the wavelength range of 200–900 nm on JASCO spectroflurometer (model: FP-8200).

Antibacterial Assay by Disc Diffusion Method

Antibacterial activities of the prepared samples were studied using disc diffusion method with two strains of bacteria such as S*taphylococcus aureus* ATCC 51740 (*S. aureus*) and *Escherichia coli* ATCC 13762 (*E. coli*), and the zone of inhibition was analyzed. The pathogenic bacteria were cultured individually on Muller-Hinton broth at 37°C for 24 h, before inoculation for assay. Solid culture was prepared by mixing 2 g of beef extract, 3.5 g of casein acid hydrolyte, and 3 g of starch in 200 mL of distilled water. A total of 100 µL of microbial culture was uniformly distributed on the plate. Sterile paper discs saturated with the solution of 100 µL for each test sample (ZnO, ZCP, ZAP, and ZSP) were gently placed over the test organism seeded plates. An Amikacin 30 µg antibiotics disc and a disc loaded with 100 µL of HCl (4N) were used as positive and negative controls, respectively. The plates were incubated for 24 h at 37°C in the bacteriological incubator. The zone of inhibition was then measured and recorded. Each experiment was made in triplicate, and the inhibition zones are given as the mean- ± standard deviation.

Antibacterial Assay by Colony Count Method

The study of the cell reduction activity of prepared samples was performed using the colony count method. With 100 µL of sample (10 mg/100 mL), an approximate number of 10^6 CFU/ml of the *S. aureus* and *E. coli* bacteria in Muller-Hinton broth was added and incubated at 37°C on a shaking platform at 250 rpm for 24 h. Control broth without the samples were also used. The number of bacterial colonies (CFU) was counted and was interpreted in terms of reduction percentage.

The percentage of microbial cell reduction (R, %) was calculated using the following equation:

$$R, \% = \frac{CFU_{control} - CFU_{sample}}{CFU_{control}} \times 100\% \quad (1)$$

where $CFU_{control}$ and CFU_{sample} are the numbers of colony-forming units per milliliter for the control and prepared samples, respectively. Each experiment was made in triplicate, and the percent reduction is given.

RESULT AND DISCUSSION

FTIR Analysis

Figure 1 shows the FTIR spectra of PTS, ZCP, ZAP, and ZSP samples. The characteristic frequencies of PTS are observed at 3423 cm^{-1} for vibration mode of O—H group, 2923 cm^{-1} and 2359 cm^{-1} due to C—H asymmetric and N—H stretching vibration, respectively. While the peaks in 1640, 1429, and 1527 cm^{-1}, which are due to the characteristics of C═O symmetric stretching vibration and N═O stretching vibration.[16] In addition, the peaks are appeared at 1100 and 1032 cm^{-1} attributed to respective guluronic acid and mannuronic acid groups.[17] Moreover, the weak sulfate band is appeared at 848 cm^{-1} (C—O—S, secondary axial sulfate) which indicates the sulfate group is located at position 4 of the fucopyranosyl residue.[18]

Because of the substitution of Zn ions, weak absorption with the considerable shift at 1640 cm^{-1} frequency and reduction in the intensity of guluronic and the mannuronic acid groups absorption frequency (1100 and 1032 cm^{-1}) is noticed in the ZCP, ZAP, and ZSP samples. In comparison with the seaweed IR spectrum, the composite's spectra displayed a new peak at 423 cm^{-1} which corresponds to Zn—O stretching vibration absorption band.[19] Further research is needed to improve the chemical interaction between the seaweed and ZnO.

X-ray Diffractrometry

Figure 2 shows the XRD patterns of the PTS, seaweed-ZnO composite, and pure ZnO. It can be seen from the figure that the XRD pattern could be assigned to hexagonal ZnO, which is

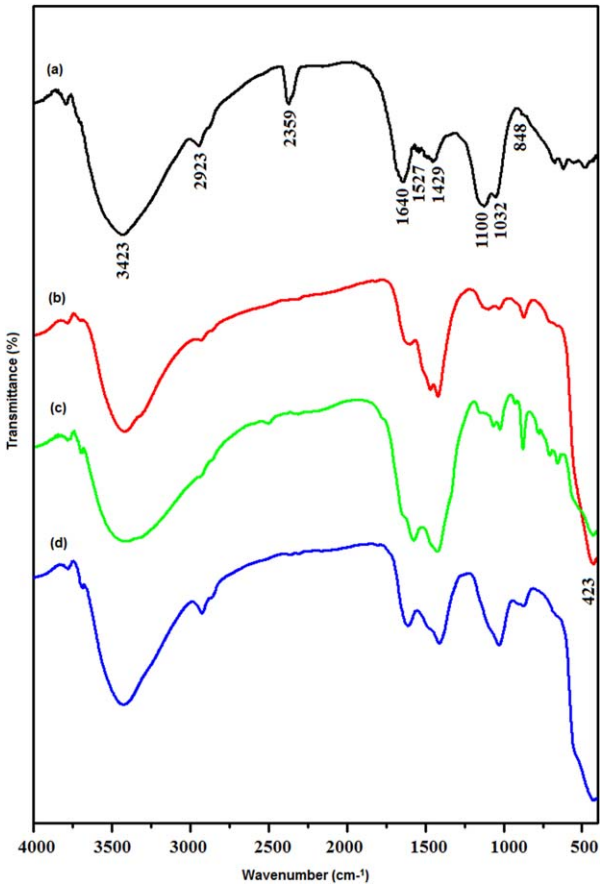

Figure 1. FTIR spectra of (a) PTS, (b) ZCP, (c) ZAP, and (d) ZSP. [Color figure can be viewed in the online issue, which is available at wileyonlinelibrary.com.]

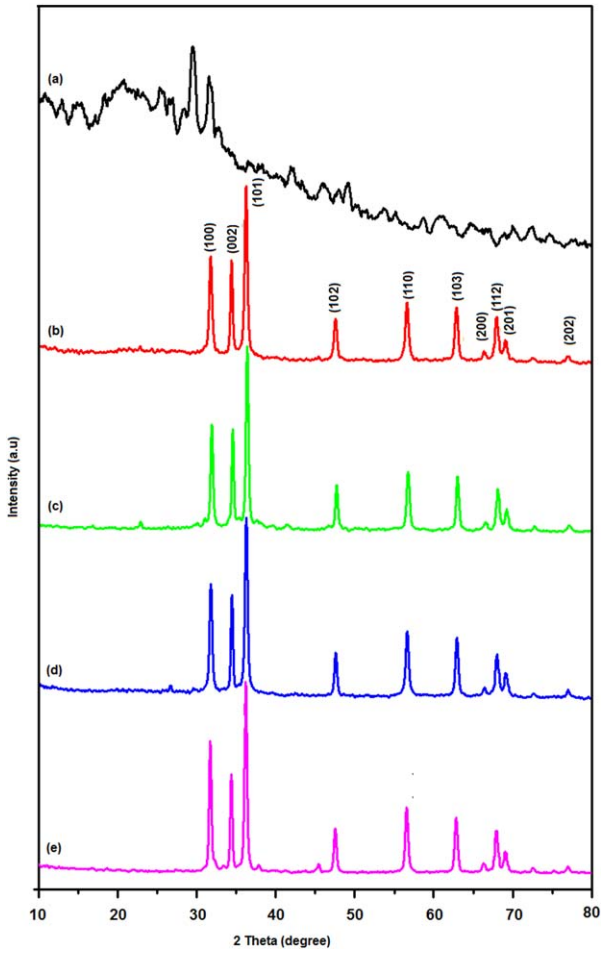

Figure 2. XRD patterns of (a) PTS, (b) ZCP, (c) ZAP, (d) ZSP, and (e) pure ZnO. [Color figure can be viewed in the online issue, which is available at wileyonlinelibrary.com.]

in good agreement with that of the standard card of JCPDS card #36–1451. The particle size calculated using the Scherer ($D = 0.94\lambda/\beta \cos\theta$) equation shows 27 nm for the ZCP sample, 28 nm for ZAP, and 29 nm for ZSP sample, respectively, which is in good agreement with the characteristic of nano-sized particles reported in literature.[20,21] No other characteristic peaks of impurities, such as $ZnCl_2$, Zn $(Ac)_2$, and $ZnSO_4$ precursor compounds are observed in these XRD patterns, and it has confirmed the high purity of synthesized product when compared with the pure ZnO nanoparticles.[21] The broad diffraction peak of PTS appeared between 15° and 30° [Figure 2(a)]. The peaks presented in the seaweed-ZnO composite are almost similar to those of the pure ZnO [Figure 2(e)] and no peaks assigned to polysaccharide were observed. This might be the content of polysaccharide layer was too small to be determined, which confirmed the result of morphological observation [Figure 3(b–d)]. The broad diffraction peak of PTS becomes weaker in presence of ZnO as reported[22,23] that the diffraction peak of PANI in the PANI/ZnO becomes weaker due to the interaction between highly crystalline ZnO nanoparticles and PANI molecules.

Surface Morphology

The surface morphology and grain size of seaweed-ZnO composite are shown in Figure 3. The change of source chemical during the preparation process results in different size and shape of the ZnO. The observed granular pattern indicated that the ZnO is predominantly grown with nano star rod shape in ZCP, ZAP, and ZSP samples. Salgado et al.[24] reported that the alginates and the fucans likely decrease the velocities of crystal growth in the corners and edges where potential planes are located, thereby causing the observed rounded calcite morphology. From above the discussions, we have to conclude that the capping with seaweed suppressed the ZnO nanocomposite growth during the reaction. Zinc sulfate results in a formation of star rod like structures with more uniform distribution than zinc chloride and zinc acetate. The star rod-like structures with uniform distribution has observed for zinc sulfate using ZnO nanocomposite growth than zinc chloride and acetate used growth of nanocomposites. This can be due to the different binding capacity of polysaccharides of zinc species arising from zinc sulfate or zinc chloride by Baskoutas et al.[14] The agglomeration of ZnO was apparent to some places with formation of Zn—O—Zn bonds between the nanocomposites due to the existence of water molecules.

The EDAX spectrum of PTS species is shown in Figure 4(a). The figure indicates that the seaweed contains many elements

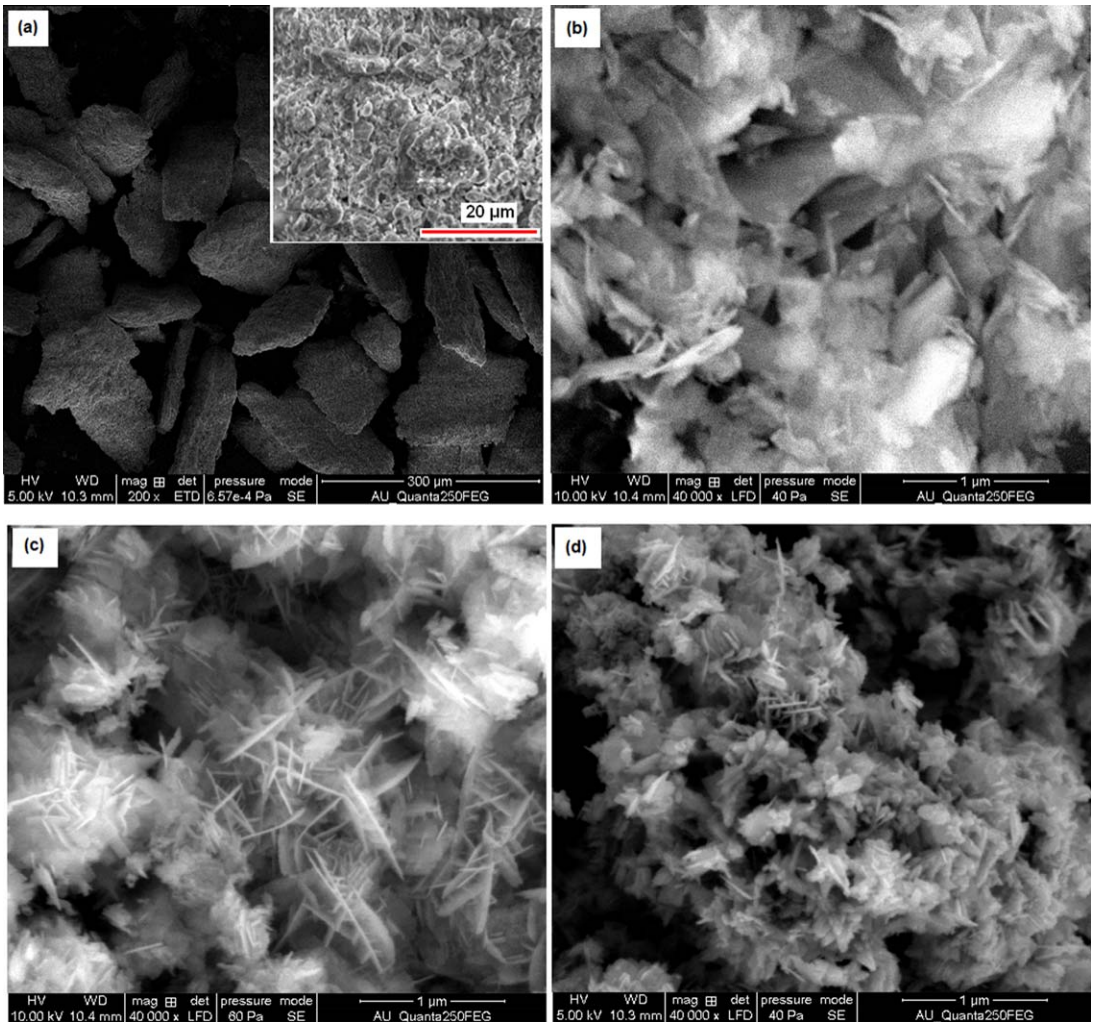

Figure 3. SEM images of (a) PTS, (b) ZCP, (c) ZAP, and (d) ZSP. [Color figure can be viewed in the online issue, which is available at wileyonlinelibrary.com.]

such as sodium, magnesium, aluminum, silicon, potassium, sulfur, chlorine, calcium, iron, carbon, and oxygen [Figure 4(a)]. The EDAX spectra of ZCP, ZAP, and ZSP samples show the Zn metal deposition on the surface of the samples [Figure 4(b–d)]. Compared with other two samples (ZCP and ZAP), the ZSP sample shows some other elements such as sulfur, chlorine, titanium, and vanadium elements [Figure 4(d)]. Since, polysaccharide consists of two active binding sites of mannuronic acid and guluronic acid [Figure 1(a)] and it is expected that these metal ions would bind to these acids on the sites of —COO— and —OH sites.[13]

TEM Analysis

TEM images of seaweed-ZnO composite are shown in Figure 5. As shown in Figure 5, the ZnO nanoparticles are almost in nanorod form with well distributed in polysaccharide composites. The length of ZnO nanorods are in the range of 113–142 nm for ZCP, 193–224 nm for ZAP and 164–169 nm for ZSP samples. The average diameter of the particle sizes are in the range of 20–40 nm, in agreement with the XRD results. From the SEM and TEM images, it can be seen that the synthesized nanorods are well dispersed. The XRD pattern and TEM images demonstrate that, with this presented simple method, the wurtzite type ZnO nanorods with small diameter and large aspect ratio can be directly synthesized. From the TEM images, it can be seen that the ZSP [Figure 5(b)] has more uniform mixing of Zn/ZnO with seaweed than ZCP [Figure 5(a)].

UV–Vis Absorption Spectra

The UV–visible spectrum is a useful technique for the characterization of semiconductor nanocomposite which exhibits a quantum size effect caused by the photogenerated electron–hole pairs. UV-Visible spectra of seaweed encapsulated ZnO nanoparticles are shown in Figure 6. The absorption spectrum of methanol dissolved PTS exhibits four absorption peaks around at 216, 266, 411, and 662 nm which is characteristic peaks of PTS. Earlier, it is reported that the excitonic absorption at 373 nm for bulk ZnO. In this study, the sharp peak is observed at 219 nm with the higher intensity of the excitation transition in surface electron for embryonic ZnO particles, and the weak absorptive peak is exhibited at 246 nm related to exciton resonant absorptive peak of ZnO nanocomposite[25] and ZnO thin

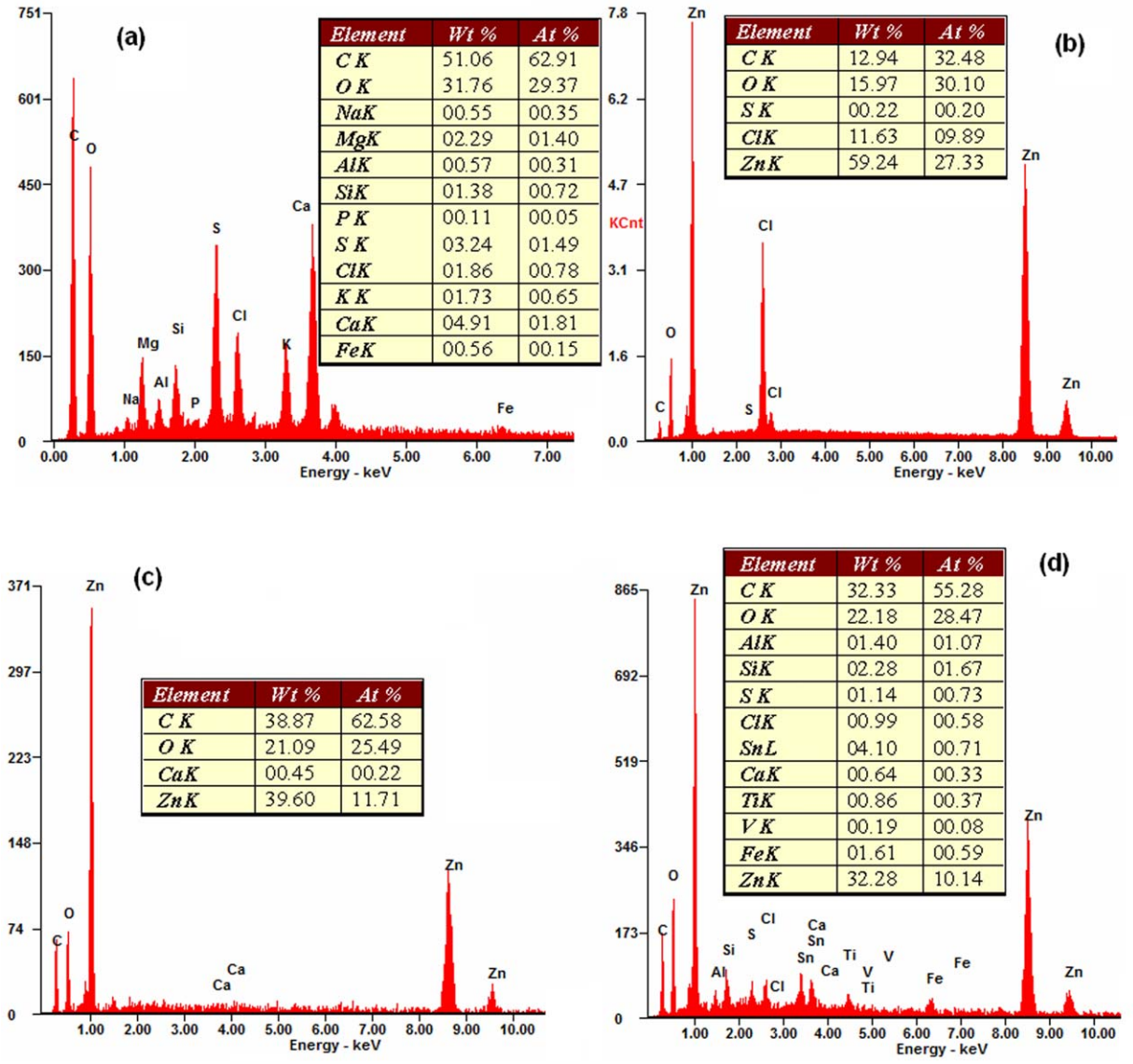

Figure 4. EDAX spectra of (a) PTS, (b) ZCP, (c) ZAP, and (d) ZSP. [Color figure can be viewed in the online issue, which is available at wileyonlinelibrary.com.]

films.[26] This may be due to a quantum confinement effect. UV absorption intensity in the 200–400 nm range for ZCP, ZAP, and ZSP sample is may be due to the presence of more nanoparticles.

Fluorescence Analysis

Room temperature FL spectra of seaweed-ZnO composite recorded with an excitation of 325 nm is shown in Figure 7. In a typical FL spectrum of ZnO, a strong UV emission peak at near band edge and broad emission peak around 450–550 nm is commonly observed.[27] Generally, blue-violet emissions of ZnO are highly desirable, and they have been great potential in light emitting and biological fluorescence labeling applications.[28] In our knowledge in earlier literature, few papers have reported in the in blue-violet region observation in ZnO, but their PL intensity is so weak for applications.[29,30] In this study, the samples ZCP, ZAP, and ZSP displays a peak at 415 nm due to the ZnO nanocomposite and a broad peak with high intensity around 380–480 nm is observed due to the blue-violet emissions.

Green emission around 450–550 nm is usually attributed to defects resulting from oxygen vacancies produced by recombination of photo-generated holes with the single ionized charge states of the defect.[31] However, in this study, the absence of the green peak suggests the concentrations of the defects responsible for the deep level emissions are negligible. Singla et al.[6] have found that the relative intensity of the emission peaks in the visible region decreased considerably by used surfactants. Surfactants play two roles to reduce the visible emission: first, they help to form defect-free nano crystals during nucleation and secondly. They attach to the surface of nanocomposite so as to keep the particle size minimal. In this study, the seaweed particles also reduced the trap emissions of the ZnO

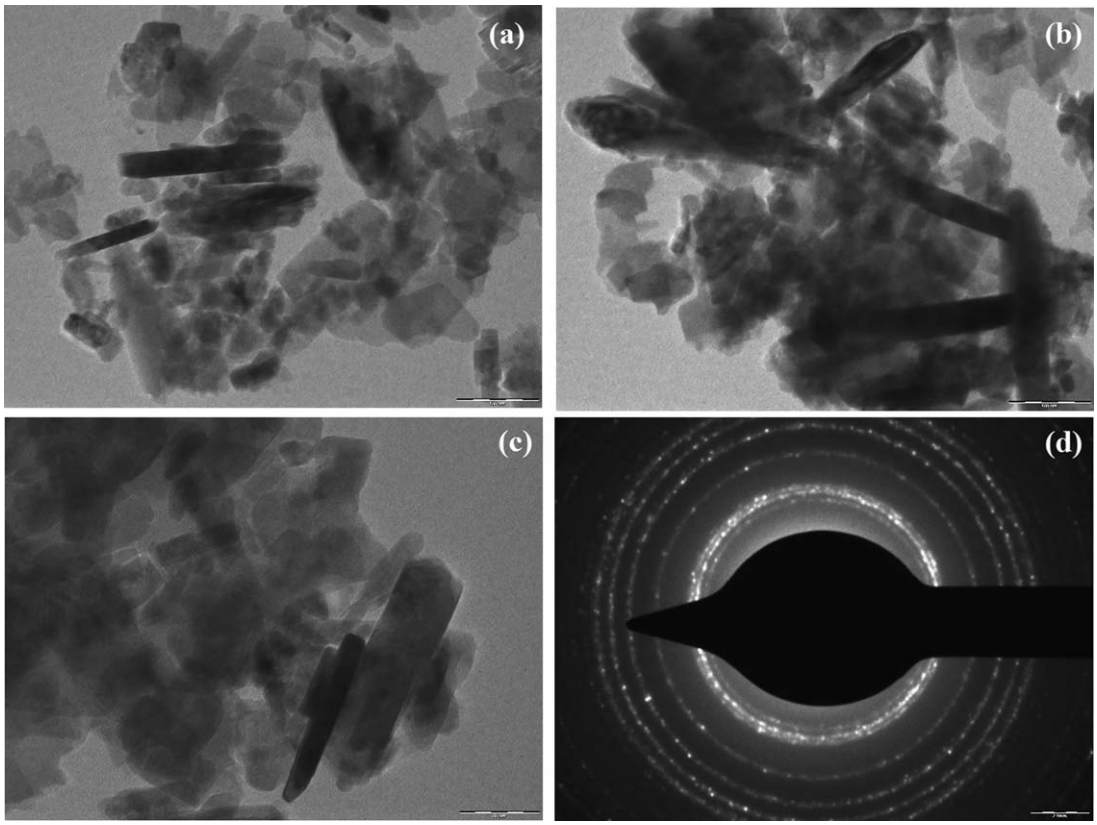

Figure 5. TEM images of (a) ZCP, (b) ZAP (c) ZSP, and (d) SAED pattern of ZCP.

nanocomposite and found that there is not much difference in the emission behavior between the ZCP, ZAP, and ZSP samples. It is concluded that, the synthesis of seaweed-ZnO composite with high UV emission in the blue-violet region, and it may be used for light emitting and biological fluorescence labeling applications.

Antibacterial Activity

ZnO nanoparticles are used as one of the effective antibacterial agents among the metal oxides against both gram-positive and -negative bacteria. Various mechanisms were proposed for the antibacterial activity of ZnO nanoparticles like generation of active oxygen species such as H_2O_2 from the surface of ZnO nanoparticles,[21,32] distort and damage caused by ZnO

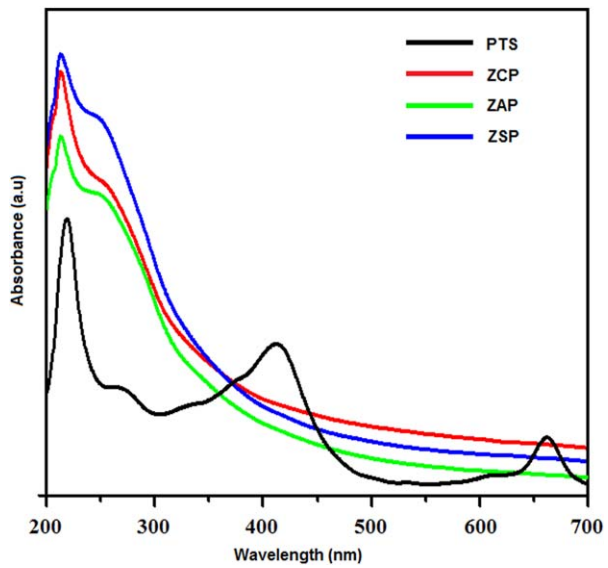

Figure 6. UV-vis spectra of PTS, ZCP, ZAP, and ZSP. [Color figure can be viewed in the online issue, which is available at wileyonlinelibrary.com.]

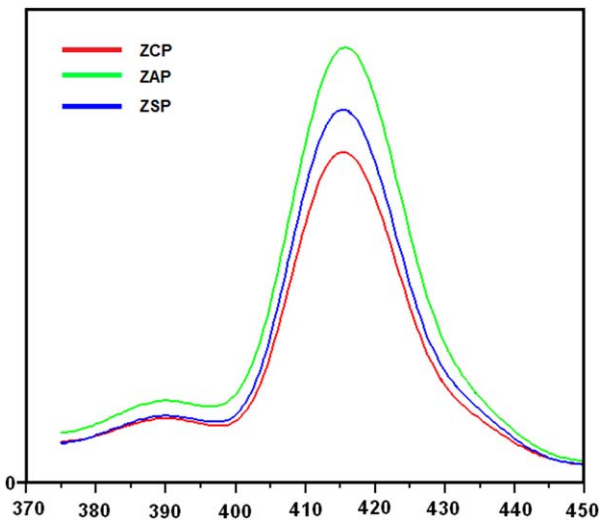

Figure 7. Fluorescence spectra of ZCP, ZAP, and ZSP. [Color figure can be viewed in the online issue, which is available at wileyonlinelibrary.com.]

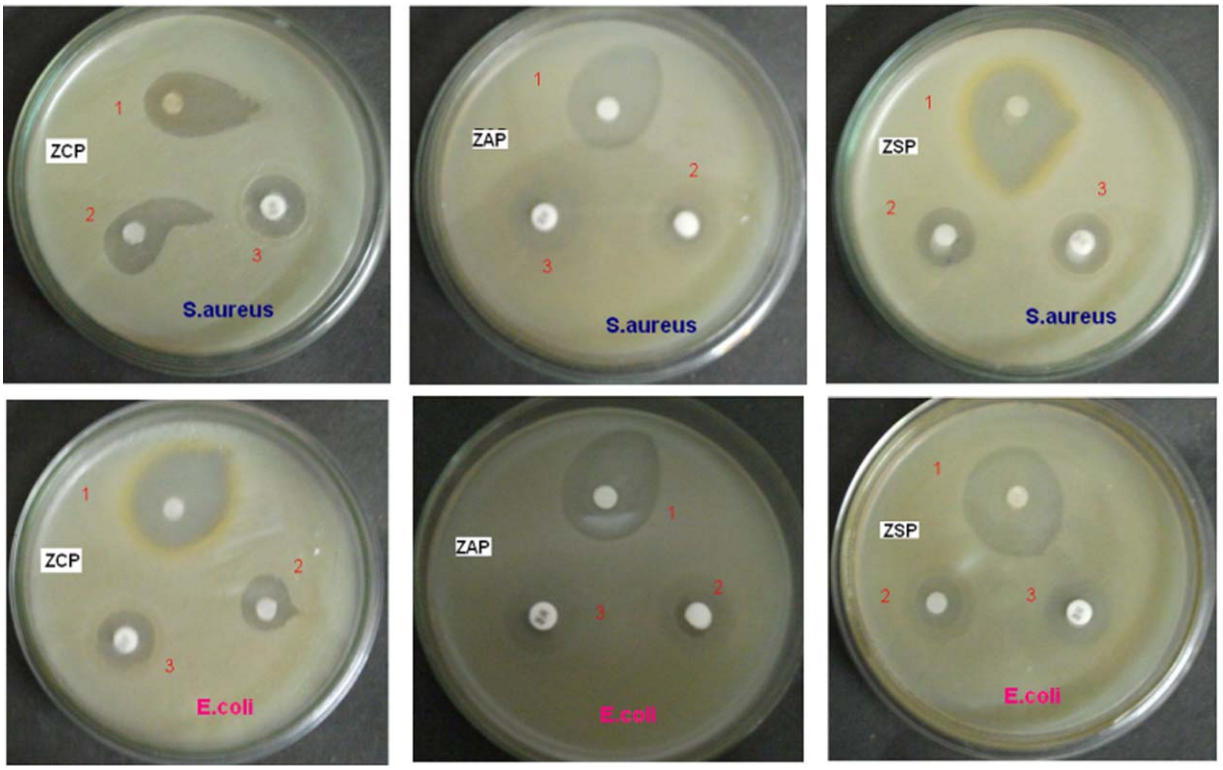

Figure 8. Zone of inhibition pictures for the ZCP, ZAP, and ZSP samples with *S.aureus* and *E.coli* bacteria. 1 = sample, 2 = positive control, and 3 = negative control. [Color figure can be viewed in the online issue, which is available at wileyonlinelibrary.com.]

nanoparticles,[33] and ZnO nanorods in the liquid phase[34] on bacterial cell membrane is due to the leakage of intracellular contents and eventually the death of bacterial cells. However, there is lacking of exact information regarding the interaction of nanoparticles with the bacterial cell wall and possible permeation of the nanoparticles into the bacterial cells.[35]

The antibacterial activity of seaweed-ZnO composites against gram +ve and gram –ve bacteria were tested using agar diffusion method (Figure 8). The zone of inhibition values and agar plate pictures for the ZnO, ZCP, ZAP, and ZSP samples are reported in Table I. PTS has antibacterial activity because of exhibited functional groups such as N—H, N═O, and C—O—S presented in the sample.[36] In a recent review, it has been pointed out that the antiviral activity of anionic polysaccharides is not merely a function of high charge density, but has distinct structural specificities of which nature of anionic groups is undoubtedly important.[10]

In this study, zinc metal/ZnO nanoparticles are incorporated in the polysaccharide of PTS (Figure 1). The functional groups of seaweeds responsible for the antibacterial activity may be easily available for reaction with the bacteria cell wall. It is observed that the inhibition value for both bacteria, ZSP is slightly higher than ZCP and ZAP (Table I).

This may be due to the higher content of Mannuronic acid in the ZSP sample as evidenced from the strong absorbance peak observed at 1029 cm^{-1} for ZSP sample (Figure 1). Seaweed-ZnO composites shows more antibacterial activity against Gram +ve bacteria than Gram –ve bacteria (Table I), as was shown by ZnO nanoparticles[37] and bioactive compound obtained by solvent extraction of seaweed.[38]

Table I. Antibacterial Activity by Disc Diffusion Method and Colony Count Method

	Inhibition zone diameter (mm)		Microbial cell reduction (*R* %)	
Sample	*S.aureus* Gram +ve	*E.coli* Gram −ve	*S.aureus* Gram +ve	*E.coli* Gram −ve
ZnO	20 ± 0.30	19 ± 0.21	81	79
ZCP	24 ± 0.42	23 ± 0.34	90	88
ZAP	26 ± 0.47	24 ± 0.38	93	91
ZSP	28 ± 0.33	25 ± 0.43	95	93

Please note that figure 8 is not cited in text. Kindly cite it as per the journal style.

The representative results of the reduction in cell viability for the *S.aureus* and *E. coli* bacteria culture are presented in Table I. Considering the results related to the antibacterial activity of prepared samples, it is evident that the bacteriostatic effect of prepared samples on the *S.aureus* is high as was observed in the zone of inhibition method (Table I). The percentage of *S.aureus* cell reduction, *R* values for ZnO, ZCP, ZAP, and ZSP samples are 79, 88, 91, and 93%, respectively. These values are slightly higher than the *E.coli* cell reduction percentage. In the zone of inhibition method and colony count method, both bacteria showed higher antibacterial activity for ZSP sample than ZCP and ZAP samples (Table I). This may be due to the presence of more number of nano rods as was evidenced from the TEM image Figure 5(c). These results are in good agreement with the recent reports that hexagonal ZnO rods showed higher cell reduction than the ZnO nanospheres.[39] From the EDAX spectrum (Figure 4) that most of the elements present in the EDAX spectrum of PTS is also appeared in the spectrum of ZSP sample, clearly indicates the presence of more PTS in the ZSP sample than the other two samples. This clearly demonstrates that the increased antibacterial activity of seaweed-ZnO composite over ZnO may be due to the presence of seaweed and ZnO nanoparticles/rods.

CONCLUSIONS

Seaweed-ZnO composite was prepared successfully without any traces of solvent. The presence of ZnO and seaweed polysaccharide was confirmed by FTIR. XRD results were indicated that the prepared ZnO nanocomposite exhibited at hexagonal wurtzite phase with good crystallinity. Surface morphology and particle size distribution of seaweed-ZnO composites were confirmed by scanning and transmission electron microscopy. The optical properties of the seaweed-ZnO composites were analyzed by UV-Visible spectroscopy. The antibacterial test showed that both samples were effective in the inhibition of *E.coli* and *S.aureus* growth. A high reduction of the number of viable cells of these two bacterial cultures after the exposure to seaweed-ZnO composites can be of great important in food package manufacturing, as well as in the process of water purification. Further research is needed to improve the chemical interaction between the seaweed polysaccharide and ZnO.

ACKNOWLEDGMENTS

The authors thank the UGC, New Delhi, for providing financial assistance to the first author under UGC-BSR Fellowship.

REFERENCES

1. Gondal, M. A.; Drmosh, Q. A.; Yamani, Z. H.; Saleh, T. A. *Appl. Surf. Sci.* **2009**, *256*, 298.
2. Li, Y. Q.; Fu, S. Y.; Mai, Y. W. *Polymer* **2006**, *47*, 2127.
3. Wang, R. H.; Xin, J. H.; Tao, X. M. *Inorg. Chem.* **2005**, *44*, 3926.
4. Iwasaki, T.; Satoh, M.; Ichio, S. *J. Mater. Process. Technol.* **2003**, *142*, 131.
5. Hu, Y.; Chen, H. J. *J. Nanopart. Res.* **2008**, *10*, 401.
6. Singla, M. L.; Muhamed Shafeeq, M.; Kumar, M. *J. Lumin.* **2009**, *129*, 434.
7. Mandal, T. K.; Fleming, M. S.; Walt, D. R. *Nano. Lett.* **2002**, *2*, 3.
8. Xiong, H. M.; Zhao, X.; Chen, J. S. *J. Phys. Chem. B.* **2001**, *105*, 10169.
9. Chew, Y. L.; Lim, Y. Y.; Omar, M.; Khoo, K. S. *LWT. Food. Sci. Tech.* **2008**, *41*, 1067.
10. Ghosh, T.; Chattopadhyay, K.; Marschall, M.; Karmakar, P.; Mandal, P.; Ray, B. *Glycobiology* **2009**, *19*, 2.
11. Mercy Sheeba, J.; Thambidurai, S. *J. Appl. Polym. Sci.* **2009**, *113*, 2287.
12. Salgado, L. T.; Andrade, L. R.; Amado Filho, G. M. *Protoplasma* **2005**, *225*, 123.
13. Sreeram, K. J.; Indumathy, R.; Rajaram, A.; Nair, B. U.; Ramasami, T. *Mater. Res. Bull.* **2006**, *41*, 1875.
14. Baskoutas, S.; Giabouranis, P.; Yannopoulos, S. N.; Dracopoulos, V.; Toth, L.; Chrissanthopoulos, A.; Bouropoulos, N. *Thin Solid Films* **2007**, *515*, 8461.
15. Carp, O.; Visinescu, D.; Patrinoiu, G.; Tirsoaga, A. *Rev. Roum. Chim.* **2011**, *56*, 901.
16. Ye, H.; Zhou, C.; Li, W.; Hu, B.; Wang, X.; Zeng, X. *Carbohydr. Polym.* **2013**, *97*, 659.
17. Pereira, L.; Sousa, A.; Coelho, H.; Amado, A. M.; Riveiro-Claro, P. J. A. *Biomol. Eng.* **2003**, *20*, 223.
18. Chizhov, A. O.; Dell, A.; Morris, H. R.; Haslam, S. M.; McDowell, R. A.; Shaskov, A. S. *Carbohydr. Res.* **1999**, *320*, 108.
19. Tang, L. G.; Hon, D.-N. S. *J. Appl. Polym. Sci.* **2001**, *79*, 1476.
20. Zhu, S.; Wei, W.; Chen, X.; Jiang, M.; Zhou, Z. *J. Solid State Chem.* **2012**, *190*, 174.
21. Nagarajan, S.; Kuppusamy, K. A. *J. Nanobiotechnol.* **2013**, *11*, 39.
22. Ameen, S.; Akhtar, M. S.; Ansari, S. G.; Yang, O.-B.; Shin, H.-S. *Superlattices Microstruct.* **2009**, *46*, 872.
23. Kannusamy, P.; Sivalingam, T. *Polym. Degrad. Stab.* **2013**, *98*, 988.
24. Salgado, L. T.; AmadoFilho, G. M.; Fernandez, M. S.; Arias, J. L.; Farina, M. *J. Cryst. Growth* **2011**, *321*, 65.
25. Chen, Q. H.; Zhang, W. G. *J. Non-Cryst. Solids* **2007**, *353*, 374.
26. Liu, Y. L.; Liu, Y. C.; Liu, Y.; Shen, D.; Lu, Y.; Zhang, J. Y.; Fan, X. W. *Phys. B* **2002**, *322*, 31.
27. Liang, Z.; Yu, X.; Lei, B.; Liu, P.; Mai, W. *J. Alloys. Compd.* **2011**, *509*, 5437.
28. Zeng, H.; Duan, G.; Li, Y.; Yang, S.; Xu, X.; Cai, W. *Adv. Func. Mater.* **2010**, *20*, 561.
29. Zeng, H.; Cai, W.; Hu, J.; Duan, G.; Liu, P.; Li, Y. *Appl. Phys. Lett.* **2006**, *88*, 171910.
30. Wu, J. J.; Liu, S. C. *Adv. Mater.* **2002**, *14*, 215.
31. Vanheusden, K.; Seager, C. H.; Warren, W. L.; Tallant, D. R.; Voigt, J. A. *Appl. Phys. Lett.* **1996**, *68*, 403.
32. Yamamoto, O. *Int. J. Inorg. Mater.* **2011**, *3*, 643.
33. Liu, Y.; He, L.; Mustapha, A.; Li, H.; Hu, Z. Q.; Lin, M. *J. Appl. Microbiol.* **2009**, *107*, 1193.

34. Tam, K. H.; DjurišicÇ, A. B.; Chan, C. M. N.; Xi, Y. Y.; Tse, C. W.; Leung, Y. H.; Chan, W. K.; Leung, F. C. C.; Au, D. W. T. *Thin Solid Films* **2008**, *516*, 6167.

35. Jiang, W.; Mashayekhi, H.; Xing, B. *Environ. Pollut.* **2009**, *157*, 1619.

36. Thambidurai, S. Kim S.-K. Eds. In Handbook of Marine Macroalgae: Biotechnology and Applied Phycology; John Wiley: England, **2011**; p 205.

37. Tayel, A. A.; El-Tras, W. F.; Moussa, S.; El-Baz, A. F.; Mahrous, H.; Salem, M. F.; Brimer, L. *J. Food Safety* **2011**, *31*, 211.

38. Tuney, I.; Cadirci, B. H.; Unal, D.; Sukatar, A. *Tur. J. Biol.* **2006**, *30*, 1.

39. StankoviÇc, A.; DimitrijeviÇc, S.; UskokoviÇc, D. *Colloid Surf. B* **2013**, *102*, 21.